Structural impact of K63 ubiquitin on yeast translocating ribosomes under oxidative stress

Ye Zhou[a,1], Panagiotis L. Kastritis[b,c,d,1,2], Shannon E. Dougherty[e], Jonathan Bouvette[f], Allen L. Hsu[f], Laura Burbaum[g], Shyamal Mosalaganti[h,i], Stefan Pfeffer[g], Wim J. H. Hagen[h], Friedrich Förster[g,j], Mario J. Borgnia[f], Christine Vogel[k], Martin Beck[h,i], Alberto Bartesaghi[a,l,m,2], and Gustavo M. Silva[e,2]

[a]Department of Computer Science, Duke University, Durham, NC 27708; [b]Interdisciplinary Research Center HALOmem, Charles Tanford Protein Center, Martin Luther University Halle-Wittenberg, 06120, Halle/Saale, Germany; [c]Institute of Biochemistry and Biotechnology, Martin Luther University Halle-Wittenberg, 06120, Halle/Saale, Germany; [d]Biozentrum, Martin Luther University Halle-Wittenberg, 06120, Halle/Saale, Germany; [e]Department of Biology, Duke University, Durham, NC 27708; [f]Department of Health and Human Services, Genome Integrity and Structural Biology Laboratory, National Institute of Environmental Health Sciences, National Institutes of Health, Durham, NC 27709; [g]Department of Molecular Structural Biology, Max-Planck Institute of Biochemistry, D-82152 Martinsried, Germany; [h]Structural and Computational Biology Unit, European Molecular Biology Laboratory, D-69117 Heidelberg, Germany; [i]Cell Biology and Biophysics Unit, European Molecular Biology Laboratory, D-69117 Heidelberg, Germany; [j]Cryo-Electron Microscopy, Bijvoet Center for Biomolecular Research, Utrecht University, 3584 CH Utrecht, The Netherlands; [k]Center for Genomics and Systems Biology, Department of Biology, New York University, New York, NY 10003; [l]Department of Biochemistry, Duke University School of Medicine, Durham, NC 27710; and [m]Department of Electrical and Computer Engineering, Duke University, Durham, NC 27708

Edited by Peter B. Moore, Yale University, New Haven, CT, and approved August 3, 2020 (received for review April 1, 2020)

Subpopulations of ribosomes are responsible for fine tuning the control of protein synthesis in dynamic environments. K63 ubiquitination of ribosomes has emerged as a new posttranslational modification that regulates protein synthesis during cellular response to oxidative stress. K63 ubiquitin, a type of ubiquitin chain that functions independently of the proteasome, modifies several sites at the surface of the ribosome, however, we lack a molecular understanding on how this modification affects ribosome structure and function. Using cryoelectron microscopy (cryo-EM), we resolved the first three-dimensional (3D) structures of K63 ubiquitinated ribosomes from oxidatively stressed yeast cells at 3.5–3.2 Å resolution. We found that K63 ubiquitinated ribosomes are also present in a polysome arrangement, similar to that observed in yeast polysomes, which we determined using cryoelectron tomography (cryo-ET). We further showed that K63 ubiquitinated ribosomes are captured uniquely at the rotated pretranslocation stage of translation elongation. In contrast, cryo-EM structures of ribosomes from mutant cells lacking K63 ubiquitin resolved at 4.4–2.7 Å showed 80S ribosomes represented in multiple states of translation, suggesting that K63 ubiquitin regulates protein synthesis at a selective stage of elongation. Among the observed structural changes, ubiquitin mediates the destabilization of proteins in the 60S P-stalk and in the 40S beak, two binding regions of the eukaryotic elongation factor eEF2. These changes would impact eEF2 function, thus, inhibiting translocation. Our findings help uncover the molecular effects of K63 ubiquitination on ribosomes, providing a model of translation control during oxidative stress, which supports elongation halt at pretranslocation.

K63 ubiquitin | ribosome | cryo-EM | oxidative stress | translation

In response to environmental changes, cells must reprogram gene expression to adapt and thrive. Rapid and efficient reprogramming of gene expression is extremely important during cellular exposure to harmful conditions, such as oxidative stress. Cells under oxidative stress regulate gene expression at the transcriptional level (1) and globally repress protein synthesis while expressing a variety of antioxidant proteins to combat the harmful effects of excessive reactive oxygen species (2–4). Regulation of gene expression at the translation level can occur at different stages of this concerted series of events, which includes translation initiation, elongation, and termination (5, 6). Although several mechanisms of translation control at the initiation stage have been extensively investigated (2, 7), the molecular mechanism regulating translation postinitiation under oxidative stress remains to be fully understood.

One of the processes capable of regulating protein synthesis in response to stress involves posttranslational modification of ribosomes by ubiquitin. Ubiquitin, which is a prevalent protein modifier traditionally linked to protein degradation (8), modifies the ribosome and alters its function by inducing a variety of signaling pathways independent of proteasomal degradation (9). We have shown previously that, in response to oxidative stress, ribosomes are heavily modified by K63 ubiquitin, a chain of ubiquitin molecules linked at its lysine 63, and that this modification rapidly occurs because of redox regulation of selective ubiquitin enzymes (10). We suggested that this redox control of translation by ubiquitin (RTU) pathway acts as a fail-safe mechanism that reduces protein production postinitiation during oxidative stress (11). To gain further understanding on the role of K63 ubiquitin in the RTU, we recently developed a mass spectrometry method to identify sites of K63 ubiquitination with single amino acid resolution (11). Using this method, we showed that ribosomes bear dozens of K63 ubiquitin sites and that the most abundant and numerous sites occur at the head of the 40S subunit, colocalizing with the decoding center of

Significance

K63 ubiquitination of ribosomes serves as a key regulator of protein production during cellular exposure to oxidative stress. Defining the structural and functional mechanisms of translation regulation would support the current understanding of critical reprogramming of eukaryotic gene expression. Our paper presents an examination of the structure of K63 ubiquitinated ribosomes, revealing that this modification structurally destabilizes proteins involved in the binding of translation factors and is required to trap ribosomes at the pretranslocation stage of translation elongation. We provide evidence for a new redox regulatory mechanism of translation in which K63 ubiquitin aids the global repression of protein synthesis and is essential for coping with the harms of oxidative stress.

Author contributions: G.M.S. conceived the project; P.L.K., C.V., M.B., A.B., and G.M.S. designed research; Y.Z., P.L.K., S.E.D., J.B., A.L.H., L.B., S.M., S.P., W.J.H.H., F.F., A.B., and G.M.S. performed research; M.J.B. contributed new reagents/analytic tools; Y.Z., P.L.K., S.E.D., L.B., S.M., S.P., W.J.H.H., F.F., C.V., M.B., A.B., and G.M.S. analyzed data; and Y.Z., C.V., A.B., and G.M.S. wrote the paper.

The authors declare no competing interest.

This article is a PNAS Direct Submission.

[1]Y.Z. and P.L.K. contributed equally to this work.

[2]To whom correspondence may be addressed. Email: panagiotis.kastritis@bct.uni-halle.de, alberto.bartesaghi@duke.edu, or gustavo.silva@duke.edu.

This article contains supporting information online at https://www.pnas.org/lookup/suppl/doi:10.1073/pnas.2005301117/-/DCSupplemental.

First published August 27, 2020.

ribosomes (11). The head of the ribosome interacts with several translation factors, messenger RNA (mRNA), and transfer RNAs (tRNAs), and among other functions, participates in the translocation of tRNA molecules through their binding sites and in the peptide bond formation during elongation (5, 12). However, little is known about whether the RTU would affect specific stages of translation elongation or termination. Ribosomal K63 ubiquitination is abundant under oxidative stress (10, 11), and the elucidation of the structural impact of this modification can provide valuable insight on its functional role in translational control during the RTU.

In recent years, numerous structural studies have used single-particle cryo-EM to understand the intricate details and modes of regulation employed during the progression of the translation cycle (13, 14). Using ubiquitin isolation methods with linkage specificity, we present structures of K63 ubiquitinated ribosomes and show that these molecules are captured at the pretranslocation stage of translation elongation during oxidative stress. In contrast, cells lacking K63 ubiquitin chains show a diversity of translation intermediates during stress, suggesting that K63 ubiquitin critically constrains pretranslocating ribosomes. Our data show that K63 ubiquitination is required to induce localized changes to the 40S–60S interface that would affect the function of the elongation factor eEF2, highlighting a new process of translation control during oxidative stress.

Results

Structural Analysis of K63 Ubiquitinated Ribosomes. To determine the structural impact of K63 ubiquitination of ribosomes, we isolated K63 ubiquitinated ribosomes under oxidative stress and imaged them using single-particle cryo-EM. Incubation of yeast cells with 0.6 mM of H_2O_2 for 30 min is sufficient to induce large accumulation of K63 ubiquitin on free 40S and 60S subunits, 80S ribosomes, and polysomes (Fig. 1*A*). Moreover, untreated cells have nearly undetectable levels of K63 ubiquitin (10), similar to what is observed for the K63R ubiquitin mutant (Fig. 1*A*), which contains a mutation that prevents the elongation of K63 ubiquitin chains. After cell disruption, K63 ubiquitinated ribosomes were isolated through pulldown using a K63 ubiquitin trap (10, 11, 15), which consists of a series of ubiquitin binding domains with high affinity for K63 ubiquitin chains (*SI Appendix*, Fig. S1*A*). Our 3D classification revealed that free 40S and 60S subunits as well as fully assembled 80S ribosomes were present among the K63 ubiquitinated particles (Fig. 1*B* and *SI Appendix*, Figs. S1*B* and S2). This finding agrees with our polysome profile analysis that shows widespread distribution of K63 ubiquitin on a variety of ribosomal species (Fig. 1*A*). Free 40S particles were abundant in the sample but did not converge into high-resolution structures likely due to their intrinsic flexibility and the presence of mixed noise particles. In contrast, the fraction of particles identified as 60S (32%) and 80S (40%) were structurally more homogeneous than the 40S, and refinement of the 80S subpopulation resulted in high-resolution reconstructions (Fig. 1*B* and *SI Appendix*, Fig. S2). Although ubiquitination of free subunits might be functionally relevant, here, we focused on the intact 80S particles, which are translating ribosomes and constitute the most abundant ribosomal class targeted by K63 ubiquitin under stress.

Our 3D classification analysis generated two main classes containing intact 80S ribosomes (Fig. 1*C* and *SI Appendix*, Fig. S2). Inspection of two-dimensional (2D) class averages shows a class of isolated monosomes (80S) and a class of ribosomes that contains additional densities adjacent to the 40S entry and exit mRNA sites (80S+) (Fig. 1*C* and *SI Appendix*, Fig. S3*A*). These additional densities in the 80+ class are consistent with the presence of neighboring ribosomes localized proximally to the main 80S particle in a polysome arrangement. Our 3D reconstruction of this 80S+ conformation showed that the adjacent densities are composed of two distinct parts resembling a 40S subunit associated with a 60S (Fig. 1*C* and *SI Appendix*, Fig. S3 *A* and *B*). The 80S+ model revealed an arrangement where the 40S subunits face each other, and the 60S subunits localize toward the outside of the high-order structure (Fig. 1*C* and *SI Appendix*, Fig. S3*B*). To confirm that these additional densities represent a polysomal conformation, we isolated yeast polysomes using profiling separation and determined their structures using cryo-ET and subtomogram averaging (*SI Appendix*, Fig. S3 *C–E*). The 3D nature of image acquisition by cryo-ET revealed that polysomes can be arranged in the same conformation obtained by the single-particle cryo-EM analysis of K63 ubiquitinated 80S ribosomes. Our cryo-ET analysis of polysomes showed a clear prevalence for the small subunits facing each other, producing a pseudohelical organization (Fig. 1*D*) that we expected to be observed in the 80S+ class. These findings support the fact that the 80S+ class is, indeed, composed of polysomes. Therefore, the combined cryo-EM/ET studies corroborate that monosomes and polysomes are present in the K63 ubiquitinated pool of ribosomes, confirming our previous analysis that assembled ribosomes were targeted by K63 ubiquitin under oxidative stress (10, 11).

We next showed that 80S particles from the polysome class converged into a 3.5-Å resolution structure of elongating ribosomes (Fig. 2*A*). The maps we obtained showed high-resolution features, such as density for individual side chains of amino acids and π–π stacking of ribosomal RNA (rRNA) bases. Although it is expected that protein synthesis would be globally repressed in response to stress, translation must still occur to produce stress-related proteins (3, 4). In this context, cells would exhibit different 80S conformation states and intermediates as thousands of ribosomes still progress through the translation cycle (13). To our surprise, K63 ubiquitinated monosomes and polysomes were highly homogenous (*SI Appendix*, Fig. S4*A*), sharing several structural features of elongating ribosomes. Among these features, we observed the ratchet 40S rotated conformation and densities for the L1 stalk and for two tRNA molecules in the decoding center (Fig. 2*B*). When we aligned K63 ubiquitinated ribosomes with previously published rotated and nonrotated structures (16), we found that K63 ubiquitinated molecules are present in the pretranslocation stage of elongation (*SI Appendix*, Fig. S4 *B* and *C*), suggesting that K63 ribosomes occupy a single and well-defined stage of translation. Translocation is a step of the elongation process characterized by a ratchet movement, a 40S–60S rotation that moves the transcript within the decoding center and the nascent polypeptide chain from the A to the P site, allowing ribosomes to accommodate another charged tRNA (13, 17). Our analysis shows that K63 ubiquitinated ribosomes were captured specifically at the pretranslocation stage 2 of translation where ribosomes are rotated and the tRNAs are present in a hybrid position with the first molecule in transition from the A to the P site and the second molecule from the P to the E site (Fig. 2*B*). This intermediate is formed prior to the binding of eEF2, a eukaryotic elongation factor required for translocation to occur.

To better understand the structural properties of K63 ubiquitinated molecules, we further classified the K63 ubiquitinated polysome particles into three subclasses. Although one of the subclasses (subclass 3) did not achieve high resolution (*SI Appendix*, Fig. S2*A*), the quality of the remaining two reconstructions allowed us to detect several structural differences between them. Polysomal subclasses 1 and 2 aligned well with translocating ribosomes (Fig. 2*C*), were present in the ratcheted state, and had tRNAs in the hybrid position (*SI Appendix*, Fig. S4*D*). When aligned to translocating ribosomes (14), the K63 polysome subclass 1 (58%) showed a 4° rotation in the 40S subunit that is not present in subclass 2 (21%) (Fig. 2*C*), a swivel-like motion that is associated with the translocation step of elongation (18). At low resolution, the three subclasses also showed differences in the position of the L1 stalk with subclass 1 presenting the L1 stalk in its closed position, while the stalk adopted the open conformation in the other two subclasses (Fig. 2*D*). The L1 stalk is a 60S structural component

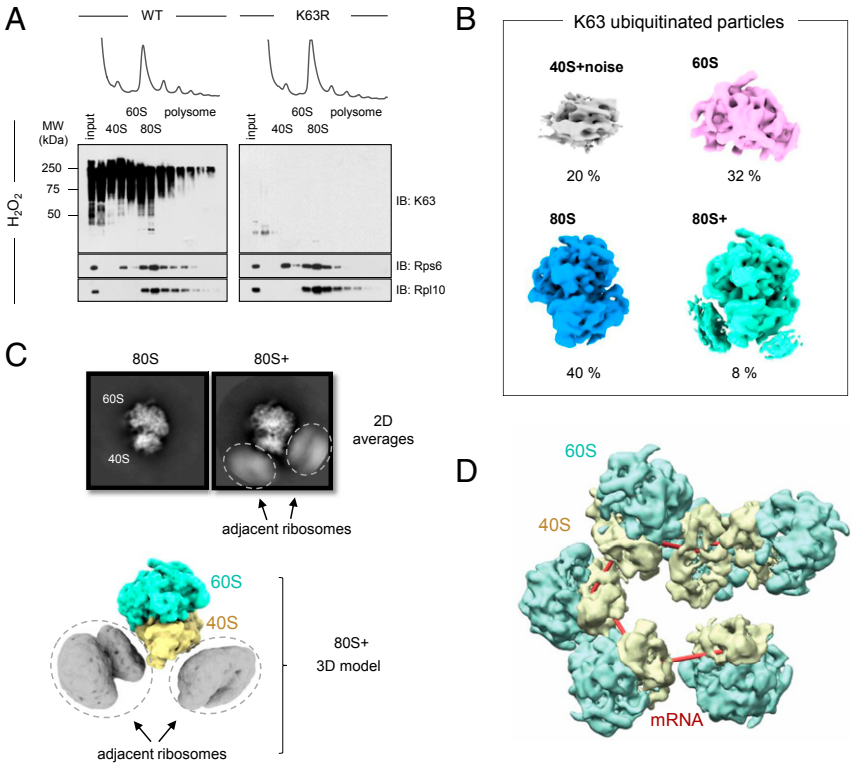

Fig. 1. K63 ubiquitin modifies ribosomes and polysomes in response to stress. (*A*) anti-K63 immunoblot (IB) of fractions from polysome profile separation of wild-type (WT) and K63R ubiquitin mutant strain under H_2O_2 stress. anti-Rps6 (eS6) and anti-Rpl10 (uL16) were used as markers for the 40S small and 60S large subunits, respectively. (*B*) A 3D classification analysis of K63 ubiquitinated ribosomes showing 40S and noise particles, 60S, 80S, and one extra 80S class containing additional densities (80S+). (*C*) The 2D class averages and 3D reconstruction for the 80S+ class highlighting density for adjacent ribosomes (dashed circles). (*D*) Subtomogram averaging reconstruction of polysomes shows relative orientation of ribosomes in a pseudohelical arrangement. The red line indicates the idealized shortest possible path of the mRNA from the entry to the exit sites.

that interacts with tRNA during translocation and assists the release of tRNA from the E site (19). Furthermore, by comparing the high-resolution polysome subclasses 1 and 2, we observed a minor shift in the position of the hybrid tRNA in the P/A position with the major subclass being slightly more advanced in the translocation process than the minor class (*SI Appendix*, Fig. S4 *D* and *E*). These results corroborate that K63 ubiquitinated polysomes occupy a restricted conformational space within the pretranslocating stage of elongation. Our previous work showed that K63 ubiquitination of ribosomes under stress impairs their capacity to produce proteins and acts postinitiation (11). Building on these previous findings, our new data suggest that K63 ubiquitin might, indeed, act postinitiation by stalling translation of both 80S monosomes and polysomes at the pretranslocation stage 2 of elongation.

K63 Ubiquitin Is Required for Conformational Changes at the Ribosomal Binding Sites for eEF2. Our published proteomics data showed that K63 ubiquitin modifies several lysine residues proximally to the ribosome decoding center (11). Here, we used the structural location of these modifications to understand how K63 ubiquitinated ribosomes are captured at pretranslocation. The 40S subunit, which is the target of multiple K63 ubiquitin sites (Fig. 3*A*), is also a highly dynamic subunit, and provides a challenging surface for molecular investigation. Although EM density for K63 ubiquitin chains was not visible in the cryo-EM maps due to expected high flexibility and likely stochasticity of ubiquitination (20), we observed that K63 ubiquitin impacts several ribosomal proteins that interact with eEF2 (Fig. 3*A*). A suboptimal interaction of K63 ubiquitinated ribosomes and eEF2 could determine ubiquitin's role in translocation.

To further investigate the role of K63 ubiquitin on eEF2 interacting proteins, we compared our K63 ubiquitinated model to unmodified translocating ribosomes (PDB ID 6GQ1) and verified that K63 ubiquitinated ribosomes show several conformational changes for proteins present at the interface of the 40S and the 60S subunits (Fig. 3*B*). Compared to unmodified ribosomes, densities for ribosomal proteins uL10 (Rpp0) and uL11 (Rpl12) were only partially detected in our cryo-EM maps, likely due to increased structural flexibility. uL10 is highly ubiquitinated under stress (11) and the presence of flexible ubiquitin chains could explain the dynamics of this protein. uL10 is an acidic protein essential for the formation of the P stalk, a pentameric structure involved in the binding of the elongation factor eEF2 and in the formation of the GTPase associated center (21–23). The C terminus of uL10 interacts with a heterotetramer of P1 and P2 to form the P stalk, while conserved rRNA loops connect uL10 to uL11 (24, 25). The map suggests that the P stalk occupies an open conformation in the presence of K63 ubiquitin (Fig. 3*B*), which is rarely observed in actively translating ribosomes (*SI Appendix*, Fig. S4*F*). Together with uL10, uL11 forms the base that stabilizes the P stalk (26), and our results show that both uL10 and uL11 are highly flexible in the K63 ubiquitinated structure. P1 and P2, the other ribosomal proteins involved in the formation of the P stalk, are intrinsically flexible containing dynamic hinges associated with their C terminus (21, 27), thus, explaining the lack of density for the $[P1\text{-}P2]_2$ structure.

Finally, we also observed higher flexibility for eL40, a 60S protein that makes a distal contact with uL10 and eEF2 (Fig. 3 *A* and *B*). As the elongation factor eEF2 binds to the 60S–40S interface, contacts with 40S proteins are also expected in addition to contacts with 60S ribosomal proteins in the P stalk (23). Two proteins in the beak of the 40S subunit, eS12 (Rps12) and eS31 (Rps31), interact with domains II and IV of eEF2 (23), and

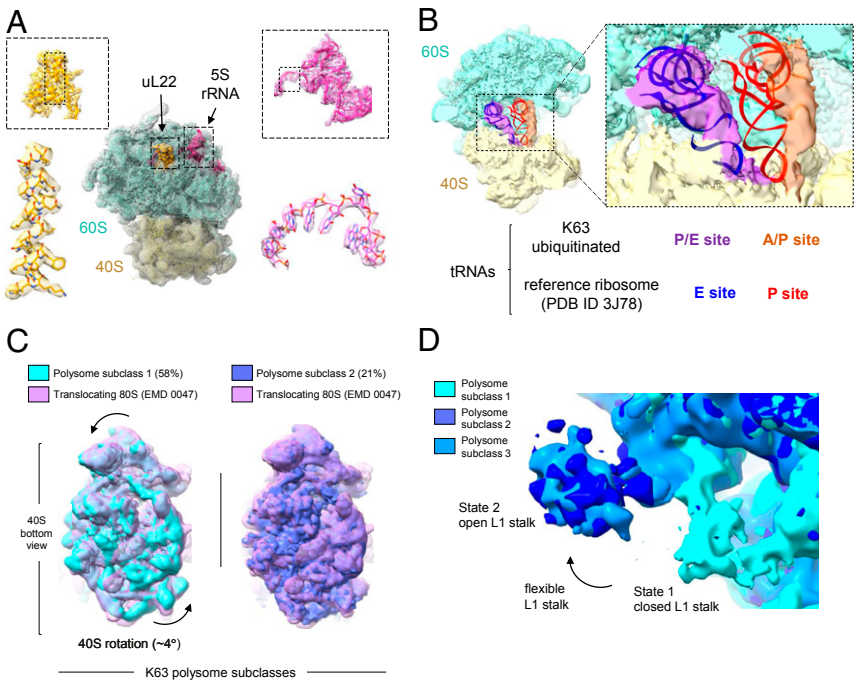

Fig. 2. K63 ubiquitinated ribosomes are captured at elongation. (*A*) Structure of the K63 ubiquitinated 80S ribosome at 3.2-Å resolution highlighting the rigid fit of uL22 (residues 85–104) and the density observed for the 5S rRNA (bases 19–24). (*B*) K63 ubiquitinated ribosomes show density for two tRNA molecules in the hybrid state A/P (orange) and P/E (purple). Rigid fit of the tRNAs from 80S ribosome (PDB ID 3J78) (16) into the EM map of ubiquitinated ribosomes showing the relative position of the P (red) and E (blue) sites. (*C*) Alignment of polysome subclasses 1 and 2 to translocating 80S ribosomes (PDB ID 6GQ1) (14). Subclass 1 shows a small rotation for the 40S subunit. (*D*) Dynamic L1 stalk presented in close conformation for subclass 1, and open conformation for subclasses 2 and 3 of K63 ubiquitinated polysomes.

inspection of these regions in the K63 ubiquitinated ribosomes also revealed increased flexibility in comparison to unmodified translocating ribosomes (Fig. 3*B*). Similar to uL10, eS12 has been shown to be highly K63 ubiquitinated in response to stress (11), suggesting that this modification impacts the structural disposition of the region. Collectively, our cryo-EM maps for K63 ubiquitinated ribosomes show high destabilization of several eEF2 binding regions, indicating that flexibility of the 40S–60S interface could result in an ineffective binding or prevention of the GTPase activity of this elongation factor. Our structural analysis provides mechanistic insight on how K63 ubiquitin could trap polysomes at elongation under stress by preventing eEF2-mediated translocation.

Although K63 ubiquitinated polysomes were captured at the pretranslocation stage of translation and showed specific structural changes related to the elongation factor eEF2, our data did not allow us to determine whether these modifications were mediated by oxidative stress, or whether K63 ubiquitin induces these changes and prevents the progression of translation past translocation. Thus, to determine the role of K63 ubiquitin in ribosomal conformational changes, we resolved the cryo-EM structures of ribosomes isolated from yeast cells containing the K63R ubiquitin mutation treated with H_2O_2. This lysine to arginine mutation allows cells to ubiquitinate protein targets but prevents the extension of K63 ubiquitin chains (28). In this context, H_2O_2 treatment would induce redox changes without the effect of K63 ubiquitin chains, thus, helping to define the impact of K63 ubiquitin in the ribosome structure. We collected and analyzed cryo-EM images from ribosomes lacking K63 ubiquitin under stress (*SI Appendix*, Figs. S5 and S6) and obtained a consensus reconstruction resolved at 2.7 Å where several high-resolution features could be visualized for ribosomal proteins and rRNA (*SI Appendix*, Fig. S6*D*). Subsequent 3D classification analysis produced one 60S class (28%) and four distinct 80S classes with no distinguishable polysomal population (Fig. 4*A* and *SI Appendix*, Fig. S5). Polysomes from the K63R mutant are known to be biologically less stable than the WT (10, 29), which could account for the lack of polysomes in the mutant sample. Among the four 80S classes of the K63R mutant, we observed: (i) ribosomes in the classic state with one tRNA in the P position (36%); (ii) ribosomes in the classic state with tRNAs in the A and P positions (14%); (iii) ribosomes in the rotated state with tRNAs in the A and P positions (11%); and (iv) ribosomes in the pretranslocation 2 stage with tRNAs in the hybrid A/P and P/E positions (11%). The percentages are based on the total number of 80S ribosomes after exclusion of empty 80S and 40S particle populations. Moreover, we confirmed that subdivision of the K63R dataset into structural classes is robust as reclassification of the images resulted in consistent particle assignments and produced the same four conformational states. The analysis also consistently revealed the presence of defined translation states, which were determined by their rotated state and the density of tRNAs within the decoding center. All these classes converged to maps in the ∼4 Å resolution range where several high-order features of 80S ribosomes were also identified (Fig. 4*A* and *SI Appendix*, Figs. S5 and S6). The fact that we observed multiple elongation intermediates suggests that K63 ubiquitin and not H_2O_2 treatment induces the accumulation of ribosome particles at the pretranslocation stage. Moreover, the pretranslocation stage 2 has lower representation in the K63R mutant population under stress (Fig. 4*A*), indicating that our analyses are not biased toward most abundant or stable ribosomal species. Our data, thus, suggest that K63 ubiquitin promotes the accumulation of assembled ribosomes and polysomes in pretranslocation 2, a well-defined stage of translation elongation.

In comparison, we observed ribosomes from the K63R ubiquitin mutant strain in many stages of translation during oxidative stress, which included a minor pretranslocating class (Fig. 4*A*). However, it remained unclear whether the changes to the eEF2 binding sites (Fig. 3*B*) required K63 ubiquitination and could,

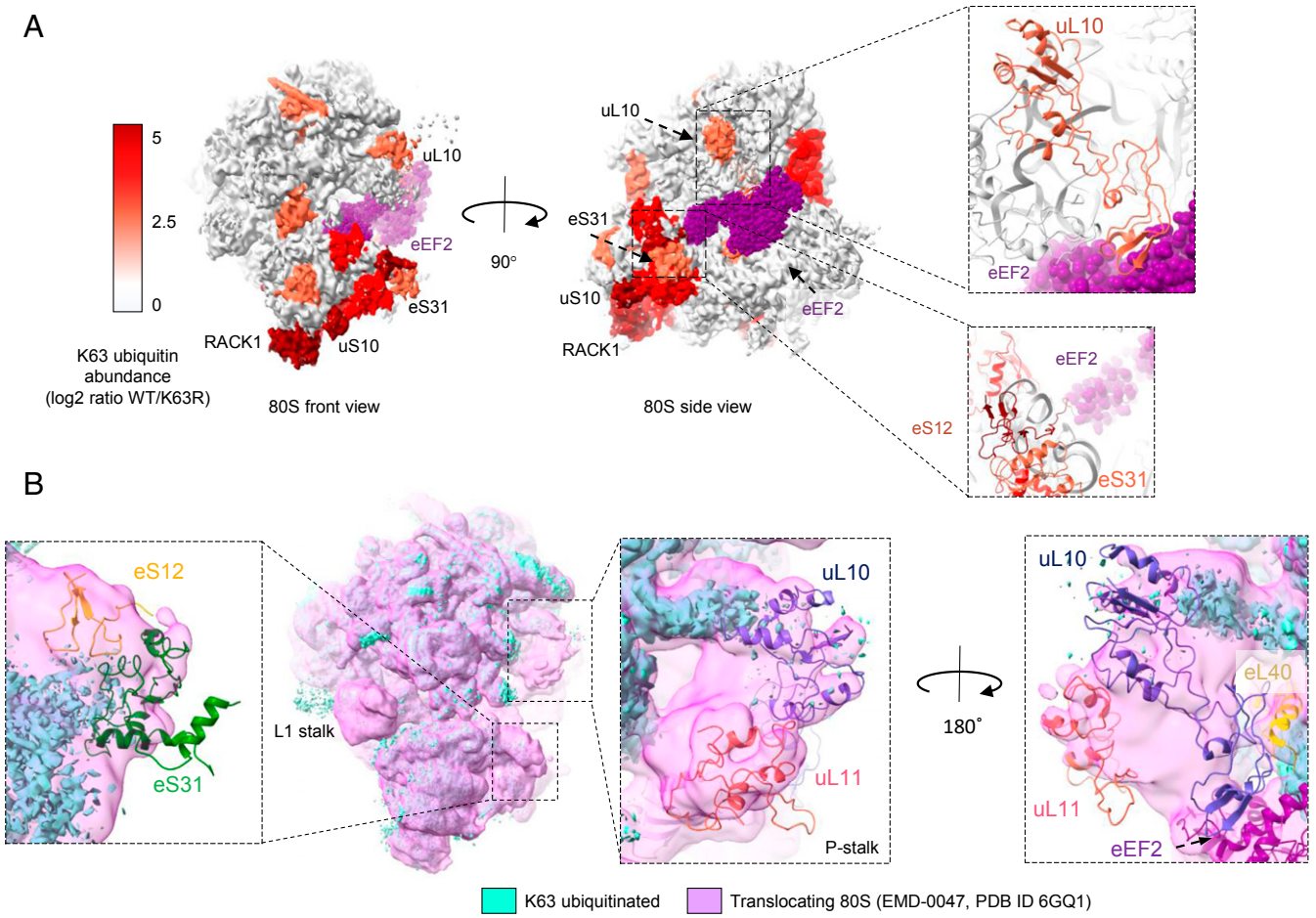

Fig. 3. Structural changes in ribosomal eEF2 binding sites. (*A*) The 80S ribosome structure (EMD-5977 and PDB ID 6GQ1) with position of the published K63 ubiquitinated proteins identified and quantified by mass spectrometry (highlighted in shades of red) (11). Abundance was determined by the quantification of peptides containing the ubiquitin remnant diglycyl lysine in the WT compared to the K63R mutants (11). The elongation factor eEF2 is depicted in purple, and insets show detailed eEF2 binding sites at the decoding center. (*B*) Alignment of maps for ubiquitinated 80S ribosomes (cyan) and translocating 80S ribosomes (PDB ID 6GQ1, pink) (14). *Insets* highlight the increased flexibility for uL10, uL11, eL40, eS12, eS31, and the P stalk in the K63 ubiquitinated maps.

therefore, prevent proper translocation. We, then, aligned the map for the K63 ubiquitinated ribosomes with the K63R mutant class at pretranslocation (Fig. 4 *B–E* and *SI Appendix*, Fig. S7). In agreement with the analysis above (Fig. 3*B*), pretranslocating ribosomes from yeast bearing the K63R mutation favors the closed conformation of the L1 stalk, which is largely open in the monosomal fraction of the K63 ubiquitinated sample (Fig. 4*B*). In addition, the structure of the K63R mutant shows a closed conformation of the P stalk (Fig. 4 *B–E*), corroborating that K63 ubiquitin is required to destabilize the P stalk under oxidative stress. Interestingly, we also identified regions where the ubiquitinated particles would display additional density when compared to the mutant (*SI Appendix*, Fig. S7*A*). In one such region, the K63 ubiquitinated structure shows a mRNA bridge of density between the uS3 (Rps3) and the 18S rRNA h16 domains, suggesting that ubiquitin could help stabilize this connection. uS3 is a ribosomal protein targeted by ubiquitin (11), which localizes by the mRNA entry channel, enhances binding of the mRNA to the 40S subunit, and supports initiation accuracy (31). Finally, we also identified the ES6a rRNA segment in the K63 ubiquitinated ribosomes that display different conformations when compared to the K63R mutant (*SI Appendix*, Fig. S7*A*), suggesting that K63 ubiquitin could induce a variety of local changes on ribosomal proteins and rRNA under stress. Consistent with our early interpretations, we proposed that the structural changes observed in the K63 ubiquitinated ribosomes are driven by the presence of K63 ubiquitin rather than by indirect effects of oxidative stress. In agreement with our model, the K63R mutant and published translocating ribosomes (14) show the same disposition for the L1 stalk and P stalk (*SI Appendix*, Fig. S7 *B* and *C*), which differ from the K63 ubiquitinated particles and reinforces the understanding that these modifications are induced by the presence of K63 ubiquitin chains. Taken together, our structural analyses indicate that K63 ubiquitination of ribosomes impacts a particular stage of the translation cycle by halting translocation due to the induction of local flexibility at the eEF2 binding sites.

Discussion

Ubiquitination of ribosomes is a widespread process, which controls translation by facilitating ribosome biogenesis, degradation, and regulatory functions, such as translation quality control and translation reprogramming (9). K63 ubiquitin modifies ribosomes and regulates protein synthesis during cellular response to oxidative stress (10, 11), however, the mechanism responsible for this regulation remains unknown. Here, we investigated the molecular mechanism behind this pathway and resolved the first structures of ribosomes modified by K63 ubiquitin during stress by cryo-EM. We show that K63 ubiquitinated monosomes and polysomes under stress are captured at the pretranslocation stage of elongation. Importantly, a one-step affinity purification of ribosomes is unlikely

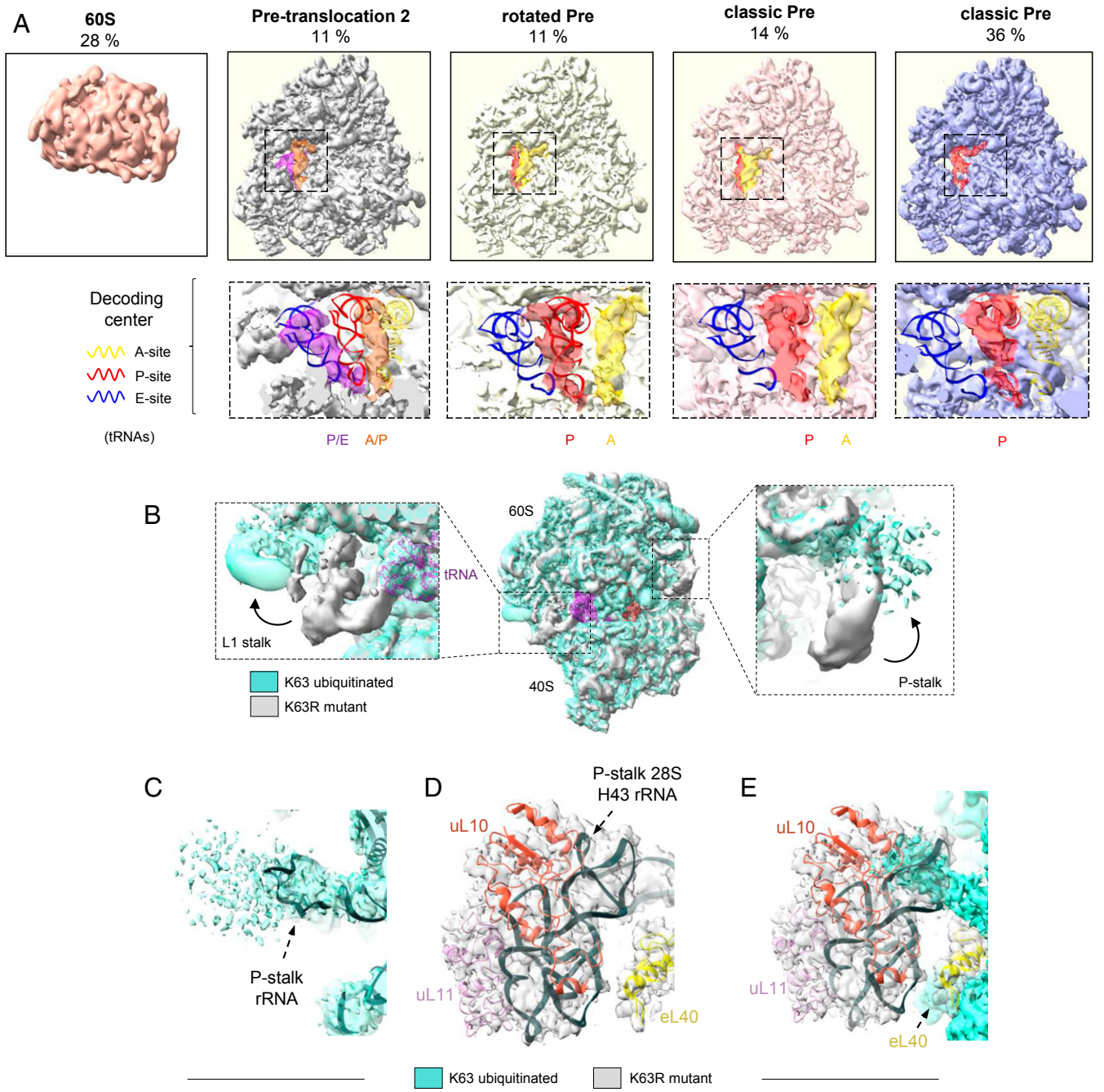

Fig. 4. Lack of K63 ubiquitin and ribosome structural changes under stress. (*A*) Ribosomes from the K63R mutant are captured at various translation stages. Inset highlights the decoding center with tRNA molecules in different positions. The A (yellow), P (red), and E (blue) sites represent the tRNA coordinates from published works (PDB ID 3J78 for the P and E sites, ref. 16 and PDB ID 4V6F for the A site) (30). (*B*) Alignment of maps for K63 ubiquitinated 80S against pretranslocating ribosomes from the K63R mutant strain. *Insets* display changes in the L1 stalk and in the P stalk. (*C–E*) Close up representation of the P stalk and fitted coordinates for uL10, uL11, and eL40. (*C*) P stalk of the K63 ubiquitinated ribosomes, (*D*) of the K63R mutant, and (*E*) of the aligned maps of K63 ubiquitinated and K63R mutant ribosomes.

to be responsible for this observed homogeneity as previous work observed substantial heterogeneity for affinity-purified ribosomes (32). Moreover, this response requires K63 polyubiquitin chains as the K63R mutant that is still able to monoubiquitinate ribosomal proteins does not reverse a range of translation phenotypes (10, 11, 29). In contrast, mutants lacking K63 ubiquitin display multiple translation intermediates indicating that K63 ubiquitin prevents the progression of elongation, leading to the accumulation of translocating ribosomes. In agreement with this interpretation, RiboSeq analyses have also revealed that oxidative stress results in accumulation of postinitiation and translocating ribosomes (3, 33). Although postinitiation control of translation has been observed during oxidative stress (2, 3), no molecular mechanism had been proposed, thus far. We have previously shown that K63 ubiquitin impacts the binding of eEF2 to ribosomes but not of eEF3 (11). Here, we speculate that the induced structural modifications control translation in an eEF2-specific manner rather than through a general mechanism of elongation regulation. Therefore, we propose a model

where K63 ubiquitin affects the dynamics of binding and dissociation of eEF2 through modification of the ribosome's P stalk and 40S beak, halting ribosome translocation (Fig. 5).

The P stalk is a multifunctional platform that recruits elongation factors, including eEF2, and stimulates their GTPase activity (21), but it is also a target of several toxins that inhibit translation (34). Recent findings proposed that available P stalks, when not engaged with elongation factors, activate Gcn2, a kinase that inactivates the eukaryotic translation initiation factor 2α (2). This activation of Gcn2 by the P stalk would, in turn, repress translation at the initiation step (35, 36). Ubiquitination of proteins in the P stalk could also provide an additional mechanism of translation inhibition by preventing the binding of elongation factors and rendering the P stalk available for Gcn2 activation, hence, participating in the integrated stress response pathway. K63 ubiquitination of proteins of the P stalk could provide new avenues to aid global inhibition of translation, and being a reversible modification, it could also act as a translation redox switch. Ubiquitination of uL10, a key protein involved in the formation of the base of the P stalk (21), could provide the initial signal for destabilization of the P-stalk structure.

Our structural analysis of ubiquitinated ribosomes also revealed that all ribosomal species, including free ribosomal subunits, can be modified by K63 ubiquitin in response to stress (Fig. 1*B* and *SI Appendix*, Fig. S2). Although some free subunits could be derived from runoff and disassembled 80S complexes, we have shown previously that individual subunits can also be modified after stress induction (10, 11). The distinct classes of 40S subunits, however, did not result in high-resolution structures (*SI Appendix*, Fig. S2). This result is expected as 40S subunits are known to exhibit higher conformational flexibility when not stabilized by initiation complexes or internal ribosome entry sites (37, 38). In addition, the lack of convergence can also be caused by the small subunit's extensive K63 ubiquitination (11). While we demonstrate that K63 ubiquitin plays an important role in elongation, K63 ubiquitin could also impact ribosome biogenesis and translation initiation. eS31 and eL40, eukaryotic ribosomal proteins fused to ubiquitin, are highly flexible in our models (Fig. 3*B*) and are important for ribosome maturation and assembly (39, 40). Although the uS3-h16 latch has been observed in arrested and terminating ribosomes (41), structural changes in uS3 could also impact initiation and binding to mRNA (*SI Appendix*, Fig. S7*A*) (31). Interestingly, the suppressor Stm1 binds to this uS3 bridge of assembled 80S particles and extends itself throughout the mRNA binding site (42). This uS3-mRNA bridge may, then, act as a translation suppressor inhibiting the relative rotation of the head and shoulder of the 40S. As ribosomes are modified by K63 ubiquitin in many additional residues during stress (11), we envision further mechanisms of translation control at the level of individual 40S and 60S subunits. While we do not expect major changes in lysine backbone, improvements in resolution and development of methods to stabilize ubiquitin chains might provide future insight on the presence and local conformation changes induced by K63 ubiquitin. While our data provide snapshots of all K63 ubiquitinated particles, it is also possible that a heterogenous subpopulation of ubiquitinated ribosomes are present in such a highly dynamic system as eukaryotic cells under stress (43, 44).

Although ubiquitination of ribosomes occurs under a variety of cellular and physiological conditions (9), the pathway of RTU, including the findings described here, has unique features that differentiate it from other pathways. RTU is triggered and depends on the oxidation of the deubiquitinating enzyme Ubp2 (10), relies on the ubiquitin enzymes Rad6 (E2) and Bre1 (E3), and regulates the translocation stage of elongation (Figs. 2 and 4). In the ribosome associated protein quality control pathway, collided ribosomes seem to serve as the surface required for the recruitment of the ubiquitin ligase Hel2/Rqt1 prior to the ubiquitination of ribosomal proteins (45, 46). Although Hel2 binds mostly to rotated ribosomes, Hel2 is present on different ribosomes classes including the nonrotated (22%), rotated state 1 (51%), and rotated state 2 (27%) (32), suggesting that different translation intermediates might serve as substrates for Hel2. We have also shown that Hel2 is not responsible for the redox accumulation of K63 ubiquitin under stress (11), suggesting that ubiquitination of ribosomes regulates different translation pathways. Therefore, our data suggest that recruitment of selective ubiquitin enzymes and the use of distinct ubiquitin linkages and lysine targets would determine the fate of ubiquitin-modified ribosomes. Our analysis uncovers molecular details by which K63 ubiquitin regulates translation postinitiation in response to oxidative stress.

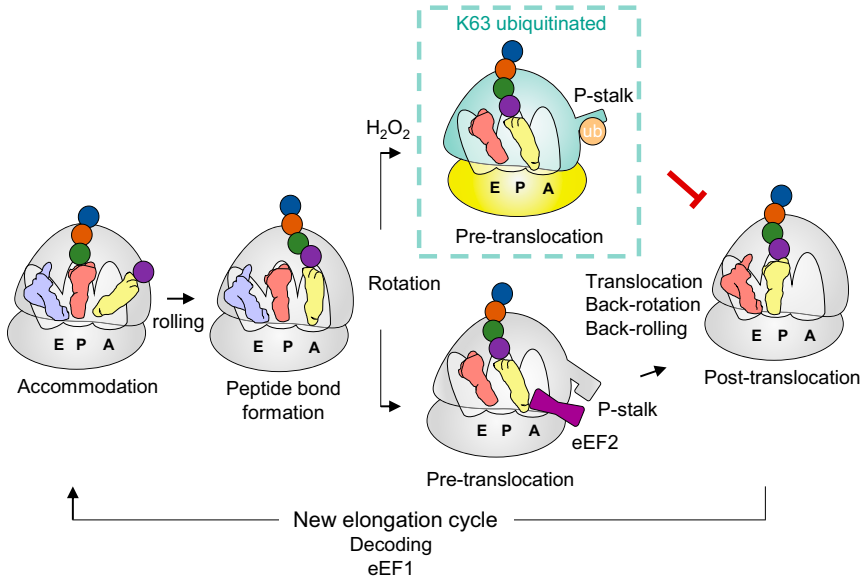

Fig. 5. Model of K63 ubiquitin translation halt in response to stress. Schematic shows the different stages of the translation cycle. K63 ubiquitination induced by oxidative stress alters the conformation of proteins in the P stalk and 40S beak, affecting the binding or activity of the elongation factor eEF2 responsible for translocation. K63 ubiquitinated ribosomes, thus, arrest at the rotated pretranslocation stage 2 of elongation.

In conclusion, our study provides a singular visualization of K63 ubiquitinated ribosomes under oxidative stress. Our results establish the foundation to understand the redox mechanisms of elongation control that have been hinted for almost 15 y (2). Our comprehensive analysis of the ubiquitinated K63R ubiquitin mutant and many states of translation underscores the impact of K63 ubiquitin on assembled ribosomes and polysomes and provides insight into the regulation of translation translocation. We propose that the overall cellular ability to cope with environmental stresses will depend on the capacity to adequately balance: (i) a transient repression of translation by K63 ubiquitin (10, 11), (ii) the synthesis of antioxidant proteins (2, 3), (iii) quality control processes (45, 46), and (iv) the degradation of excessive or damaged ribosome particles (47, 48). Many of these processes depend intimately on ribosome ubiquitination, the linkage types used, and the ubiquitin enzymes responsible for the conjugation reaction. Understanding the functional role of individual subpopulations of ubiquitinated ribosomes has the potential to establish ubiquitin as a master regulator of protein synthesis under stress. Oxidative stress and accumulation of protein ubiquitination are hallmarks of a variety of diseases (49, 50), and the control of fundamental processes in cell biology, such as translation, could provide new avenues for therapies and modes to increase cellular health.

Materials and Methods

Isolation of K63 Ubiquitinated Ribosomes. The isolation of K63 ubiquitinated ribosomes was conducted based on protocols used in our previous studies (10, 11) with minor modifications. Yeast *Saccharomyces cerevisiae* cells strain SUB280 (51) were grown to the midlogarithmic phase (optical density$_{600}$ [OD_{600}] ~0.5) in 2.4 L of minimal medium containing 0.67% yeast nitrogen base, 2% dextrose, and required amino acids at 30 °C. Cells were treated with 0.6-mM H_2O_2 for 30 min to induce oxidative stress and accumulation of K63 ubiquitin chains. Yeast cells were disrupted by bead beating in lysis buffer containing 50-mM 2-amino-2-hydroxymethyl-1,3-propanediol (Tris)·HCl pH 7.5, 100-mM KCl, 20-mM $MgCl_2$, 10% sucrose, 20-mM iodoacetamide, a cOmplete mini (ethylenedinitrilo)tetraacetic acid (EDTA)-free protease inhibitor kit (Roche), and 50 nM of FLAG K63-tandem ubiquitin binding entities; LifeSensors, catalog no. UM604). Lysate was cleared by centrifugation and loaded into a column containing M2 anti-FLAG resin (Sigma-Aldrich). The sample was eluted with 100 μg/mL of 3×-FLAG peptide (Sigma-Aldrich) in buffer containing 50-mM Tris·HCl pH 7.5, 100-mM KCl, 5-mM $MgCl_2$, and 10% glycerol. Enrichment for large complexes and sample concentration prior to cryo-EM analysis was performed using Amicon centrifugal filter units with 100-kDa cutoff.

Polysome Analysis. Polysome profiling was performed as described previously (11). Briefly, cell lysis was performed in 50-mM Tris-acetate pH 7.0 buffer containing 150-mM NaCl, 15-mM $MgCl_2$, 20-mM iodoacetamide, 0.15-mg/mL cycloheximide, 0.2-mg/mL heparin, and a cOmplete mini EDTA-free protease inhibitor kit (Roche). A total of 400 μg of RNA was sedimented by ultracentrifugation in a 7–47% sucrose gradient for 150 min at 38,000 rpm (Beckman Coulter SW41Ti rotor) at 4 °C. Gradients were fractionated from top to bottom using a Brandel density gradient fractionator system, and data were collected using Peak Chart software. Protein was precipitated with 10% tricarboxylic acid and washed with ice-cold 100% acetone prior to immunoblotting. Immunoblot was performed in poly(vinylidene difluoride) membranes using anti-K63 ubiquitin antibody at 1:6,000 dilution (EMD Millipore, catalog nos. 05–1308, clone apu3); anti-Rps10 at 1:6,000 (Sigma-Aldrich, catalog no. WH0004736M1); and anti-Rps6 at 1:4,000 (Abcam catalog no. ab40820).

Isolation of Yeast Polysomes. W303 yeast cells were grown in YPD until OD_{600} of ~0.6 and treated with 0.1-mg/mL cycloheximide for 10 min on ice. Cells were pelleted and resuspended in polysome buffer (20-mM 4-(2-hydroxyethyl)-1-piperazineethanesulfonic acid, pH 7.4, 10-mM $MgCl_2$, 150-mM KCl, 1-mM dithiothreitol, and 0.1-mg/mL cycloheximide) for lysis. To enrich for polysomes, cleared lysates (13.2 OD_{260} equivalent) were loaded onto 10–50% sucrose gradients prepared in polysome buffer and centrifuged for 90 min at 220,000× g (Beckman Coulter SW41Ti rotor). Gradients were fractionated from top to bottom using a Gradient Master system (Biocomp) while monitoring absorbance at 260 nm. Based on the acquired absorption profile (polysome profile), a gradient fraction expected to contain polysomes with, at least, five ribosomes was used for subsequent cryo-ET analysis.

Isolation of Ribosomes from the K63R Mutant Strain. Yeast *S. cerevisiae* cells from the the SUB413 (K63R) (28) strain were grown to midlogarithmic phase (OD_{600} ~0.5) in 200 mL of minimal medium containing 0.67% yeast nitrogen base, 2% dextrose, and required amino acids at 30 °C. Cells were treated with 0.6-mM H_2O_2 for 30 min to induce oxidative stress. Yeast cells were disrupted by bead beating in lysis buffer containing 50-mM Tris-acetate pH 7.0, 50-mM NaCl, 15-mM $MgCl_2$, 20-mM iodoacetamide, and a complete EDTA-free protease inhibitor kit (Roche). Lysate was cleared by centrifugation and loaded onto buffered sucrose cushion containing 50% sucrose, 50-mM Tris-acetate pH 7.0, and 15-mM $MgCl_2$. The sample was pelleted by centrifugation at 70,000 rpm for 2 h at 4 °C in a Beckman Optima Max TL ultracentrifuge using a TLA110 rotor. Ribosome pellets were resuspended in buffer containing 50-mM Tris·HCl pH 7.5, 100-mM KCl, 10-mM $MgCl_2$, and 10% glycerol.

Cryo-EM Sample Preparation and Data Collection.

K63 ubiquitinated ribosomes. Approximately 0.3 mg/mL of the sample was applied to carbon-coated holey grids (Quantifoil R2/1). Grids were glow discharged for 15 s using a Plasma Cleaner (PDC-3XG, Harrick, Ithaca, USA). Excess sample was removed by blotting for 2.5 s, and grids were plunged frozen into liquid ethane (−182 °C) using a FEI Vitrobot (Mark II) operated at 95% humidity and a temperature of 4 °C. Micrographs were recorded under low-dose conditions on a FEI Titan Krios electron microscope (Thermo Fisher Scientific) equipped with a FEI Direct detector Falcon 2 camera operated in movie mode using the EPU software. A single hole was targeted per stage movement, and one shot was used per hole. Seven frames at a nominal pixel size of 1.36 Å were collected per movie. The cumulative electron dose was 25 $e^-/Å^2$, and 5,243 movies (4,096 × 4,096, bin 1) were collected in total.

K63R mutant ribosomes. A 3-μL aliquot of the sample at a concentration of 1 mg/mL was applied onto gold grids (UltrAuFoil R1.2/1.3 300 mesh, Quantifoil Micro Tools GmbH). Grids were previously glow discharged for 30 s at 15 mA (PELCO easiGlow, Ted Pella, Inc.). Excess sample was removed by blotting for 3 s using filter paper (Whatman no. 1), and grids were plunged frozen into liquid ethane (−182 °C) using a vitrification robot (EM GP2, Leica Microsystems). Cryo-EM imaging was performed on a FEI Titan Krios electron microscope equipped with a Gatan K3 detector operated in counting mode with a calibrated physical pixel size of 1.07 Å with a defocus range between −1.0 and −3.5 μm using the Latitude S software (Gatan, Inc., Pleasanton, CA). The microscope was operated at 300 kV and aligned for parallel illumination. Six holes were targeted per stage movement, one shot per hole. No energy filter or Cs corrector was installed on the microscope. The dose rate used was ~15.0 $e^-\ Å^{-2}\ s^{-1}$ to ensure operation in the linear range of the detector. The total exposure time was 4 s, and intermediate frames were recorded every 0.067 s giving an accumulated dose of ~60 $e^-/Å^2$ and a total of 60 frames per movie. A total of 3,138 movies (5,760 × 4,092, bin 1) were collected.

Single-Particle Cryo-EM Data Processing. For the K63 ubiquitinated ribosomes dataset, movie alignment was performed in RELION (52), and the contrast transfer function was determined on the motion corrected sum of frames using CTFFIND4.1 (53). Ribosome particles were boxed out using template-free particle picking. Two consecutive rounds of 2D classification were performed to clean the extracted particles. A total of 393,353 clean particles were used for further processing (see *SI Appendix*, Fig. S2 for details). An ab initio 3D reference was generated using cryoSPARC (54). The rest of the data processing was performed in RELION. The initial 3D classification was performed using 3× binned particles. The 3D classification into 10 classes identified five distinct conformations as follows: tRNA bound 80S polysome (80S+), tRNA bound mono-80S, and empty 80S, 60S, and 40S. Particle images corresponding to the 80S+ conformation were reextracted without binning and further refined to ~4-Å resolution followed by contrast transfer function (CTF) refinement and particle polishing, which improved the resolution to 3.5 Å. The empty 80S subclasses were combined, and the corresponding particles reextracted using a binning factor of 2, followed by 3D refinement. Two additional rounds of 3D classification (without alignment) using a soft shape mask were conducted resulting in the identification of ~53,000 additional particles corresponding to the tRNA-bound mono-80S conformation from the empty 80S class. These particles were, then, combined with the previously identified tRNA-bound mono-80S group (*SI Appendix*, Fig. S2) and further refined to 3.2-Å resolution after CTF refinement and particle polishing. Empty ribosomes were not included in the final quantification of occupancy percentages.

For the K63R mutant dataset, 232,124 clean particles were identified using the same protocol described above. A high-resolution consensus reconstruction (without 3D classification) was produced using automated particle sorting (55), per-particle drift correction, CTF correction, and data-driven

dose weighting (56), resulting in a map at 2.7-Å resolution (*SI Appendix*, Fig. S6 *D* and *E*). Six classes were, then, assigned during 3D classification using 3× binned particles. No polysomal class was observed, and all of the 80S classes were combined and further refined. A 3D classification without alignment was conducted to generate four subclasses. Based on particle numbers and map quality, especially the 40S region, two subclasses were selected to perform further refinement using 2× binned particles. One more round of 3D classification was performed for the minor class, and two subclasses were refined to 3.6-Å (80S with tRNA in P site) and 4.3-Å resolutions (80S in the classic state with tRNAs in the P, A sites), respectively, using unbinned particles. For the major class, two more 3D classification rounds without alignment were performed to sort out the other two subclasses. These were, in turn, refined to 4.4-Å (80S in the rotated state with tRNAs in P, A sites) and 4.2-Å resolutions (80S with tRNAs in A/P, P/E sites), respectively. To confirm the final particle assignments, an independent run of 3D classification was executed which resulted in the same final four conformations with percentage particle overlaps of 95%, 97%, 72%, and 87%, respectively. A summary of all of the cryo-EM data and maps produced in this study are included in *SI Appendix*, Table S1.

Cryo-ET Sample Preparation and Subtomogram Averaging of Yeast Polysomes. Polysomes were loaded onto lacey carbon molybdenum grids (Ted Pella), 10-nm colloidal gold fiducials were added, and the sample was vitrified using an FEI Vitrobot (Mark IV). Single-axis tilt series were acquired on a FEI Titan Krios transmission electron microscope (TEM) (Thermo Fisher Scientific) equipped with a K2 Summit direct electron detector (Gatan, Inc., Pleasanton, CA), operated in movie mode with five to seven frames per projection image. The TEM was operated at an acceleration voltage of 300 kV, a nominal defocus of −4 μm, and 53,000× magnification (2.62-Å pixel size). Some 47 tilt series were recorded from −60 to 60° (first half: 20 to −60°; second half: 22 to 60°) with an angular increment of 2° and a total electron dose of 80–100 e^-/A^2 using the Serial EM acquisition software (57). Slit width of the Gatan imaging filter was 20 eV, zero loss. No Cs corrector was used. Frames from the K2 direct electron detector were aligned using in-house developed motion correction software based on the algorithm previously published (58). Correction of phase reversals due to the CTF was performed using MATLAB scripts and PyTom (59) on single projections (60). Tilt series were aligned by interactively located gold fiducials and reconstructed (voxel size: 2.1 nm) by weighted backprojection using the TOM-software package (61). Ribosomes were localized by template matching against a subtomogram average of the yeast 80S ribosome (62) and visual inspection of tomogram areas corresponding to peaks of the resulting cross-correlation function using PyTom and the AV3 software package (63). Subtomograms centered at the retained coordinates were individually reconstructed from the weighted aligned projections using AV3 (voxel size: 0.262 nm) and iteratively aligned using PyTom until convergence. A total of 7,125 subtomograms were used for the final polysome structure. For visualization of polysomal arrangements observed in the tomograms, the subtomogram average was replicated in a volume using the positions and orientations obtained by template matching. A model was generated after superposition of the subtomogram average on outer densities, replicating the preferred neighbor configurations five times and placing 80S into extrapolated coordinates and angles (64). The putative pathway of interconnecting polysomal mRNA was interpolated based on the positions of mRNA entry and exit sites of adjacent ribosomes.

Atomic Model Refinement. Coordinates for the yeast 80S ribosome (PDB ID 6GQ1) (14) were rigidly fit into the density maps of K63 ubiquitinated ribosomes and the K63R ubiquitin mutant using UCSF Chimera X (65), subsequently, refined with coot (66) and subjected to real space refinement in PHENIX (67). Validation statistics for both models are included in *SI Appendix*, Table S1.

Data Availability. EM maps and structural data were deposited in the Electron Microscopy Data Bank (EMDB), https://www.ebi.ac.uk/pdbe/emdb/ and the Protein Data Bank (PDB), http://www.wwpdb.org/ databases for the 3.2-Å K63 ubiquitinated 80S ribosome (accession no. EMD-22198) (68), the 4.2-Å K63R mutant in its pretranslocated state (accession no. EMD-22196) (69), and corresponding atomic models [PDB ID codes 6XIR (70) and 6XIQ (71), respectively]. The 2.7-Å consensus EM map for the K63R mutant (accession no. EMD-22197) (72) and the subtomogram averaging map (accession no. EMD-22190) (73) were also deposited in the EMDB.

ACKNOWLEDGMENTS. We are indebted to Robin Stanley for her critical evaluation of our paper. We thank M. DeLong, C. Kneifel, M. Newton, V. Orlikowski, T. Milledge, and D. Lane from the Duke Office of Information Technology and Research Computing for providing assistance with the computing environment. This work was supported, in part, by the US National Institutes of Health R00 Award ES025835 (G.M.S.). We are grateful for the support by EMBL's Electron Microscopy Core Facility. P.L.K. and S.M. acknowledge funding from Marie Curie Actions for an EMBL Interdisciplinary Postdoctoral fellowship. M.B. acknowledges funding by EMBL. C.V. acknowledges funding by the National Institutes of Health (Grant R35 GM127089) and the Zegar Family Foundation for Genomics Research at New York University. This work was supported in part by Intramural Research Program of the NIH; National Institute of Environmental Health Sciences Grant ZIC ES103326 (M.J.B.). This work was performed, in part, at the Duke University Shared Materials Instrumentation Facility (SMIF), a member of the North Carolina Research Triangle Nanotechnology Network (RTNN), which is supported by the National Science Foundation (Grant ECCS-1542015) as part of the National Nanotechnology Coordinated Infrastructure (NNCI). This study utilized the computational resources offered by Duke Research Computing (https://rc.duke.edu/).

1. A. P. Gasch *et al*., Genomic expression programs in the response of yeast cells to environmental changes. *Mol. Biol. Cell* **11**, 4241–4257 (2000).
2. D. Shenton *et al*., Global translational responses to oxidative stress impact upon multiple levels of protein synthesis. *J. Biol. Chem.* **281**, 29011–29021 (2006).
3. M. V. Gerashchenko, A. V. Lobanov, V. N. Gladyshev, Genome-wide ribosome profiling reveals complex translational regulation in response to oxidative stress. *Proc. Natl. Acad. Sci. U.S.A.* **109**, 17394–17399 (2012).
4. C. Vogel, G. M. Silva, E. M. Marcotte, Protein expression regulation under oxidative stress. *Mol. Cell. Proteomics* **10**, 009217 (2011).
5. J. W. B. Hershey, N. Sonenberg, M. B. Mathews, Principles of translational control. *Cold Spring Harb. Perspect. Biol.* **11**, a032607 (2019).
6. C. M. Grant, Regulation of translation by hydrogen peroxide. *Antioxid. Redox Signal.* **15**, 191–203 (2011).
7. B. Liu, S. B. Qian, Translational reprogramming in cellular stress response. *Wiley Interdiscip. Rev. RNA* **5**, 301–315 (2014).
8. R. Yau, M. Rape, The increasing complexity of the ubiquitin code. *Nat. Cell Biol.* **18**, 579–586 (2016).
9. S. E. Dougherty, A. O. Maduka, T. Inada, G. M. Silva, Expanding role of ubiquitin in translational control. *Int. J. Mol. Sci.* **21**, E1151 (2020).
10. G. M. Silva, D. Finley, C. Vogel, K63 polyubiquitination is a new modulator of the oxidative stress response. *Nat. Struct. Mol. Biol.* **22**, 116–123 (2015).
11. S. Back, A. W. Gorman, C. Vogel, G. M. Silva, Site-specific K63 ubiquitinomics provides insights into translation regulation under stress. *J. Proteome Res.* **18**, 309–318 (2019).
12. A. Ben-Shem *et al*., The structure of the eukaryotic ribosome at 3.0 Å resolution. *Science* **334**, 1524–1529 (2011).
13. E. Behrmann *et al*., Structural snapshots of actively translating human ribosomes. *Cell* **161**, 845–857 (2015).
14. S. Pellegrino *et al*., Structural insights into the role of diphthamide on elongation factor 2 in mRNA reading-frame maintenance. *J. Mol. Biol.* **430**, 2677–2687 (2018).
15. R. Hjerpe *et al*., Efficient protection and isolation of ubiquitylated proteins using tandem ubiquitin-binding entities. *EMBO Rep.* **10**, 1250–1258 (2009).
16. E. Svidritskiy, A. F. Brilot, C. S. Koh, N. Grigorieff, A. A. Korostelev, Structures of yeast 80S ribosome-tRNA complexes in the rotated and nonrotated conformations. *Structure* **22**, 1210–1218 (2014).
17. C. M. Spahn *et al*., Domain movements of elongation factor eEF2 and the eukaryotic 80S ribosome facilitate tRNA translocation. *EMBO J.* **23**, 1008–1019 (2004).
18. A. H. Ratje *et al*., Head swivel on the ribosome facilitates translocation by means of intra-subunit tRNA hybrid sites. *Nature* **468**, 713–716 (2010).
19. J. Fei, P. Kosuri, D. D. MacDougall, R. L. Gonzalez Jr., Coupling of ribosomal L1 stalk and tRNA dynamics during translation elongation. *Mol. Cell* **30**, 348–359 (2008).
20. L. Chang, Z. Zhang, J. Yang, S. H. McLaughlin, D. Barford, Atomic structure of the APC/C and its mechanism of protein ubiquitination. *Nature* **522**, 450–454 (2015).
21. P. Gonzalo, J. P. Reboud, The puzzling lateral flexible stalk of the ribosome. *Biol. Cell* **95**, 179–193 (2003).
22. T. Naganuma *et al*., Structural basis for translation factor recruitment to the eukaryotic/archaeal ribosomes. *J. Biol. Chem.* **285**, 4747–4756 (2010).
23. A. M. Anger *et al*., Structures of the human and Drosophila 80S ribosome. *Nature* **497**, 80–85 (2013).
24. C. Santos, J. P. Ballesta, The highly conserved protein P0 carboxyl end is essential for ribosome activity only in the absence of proteins P1 and P2. *J. Biol. Chem.* **270**, 20608–20614 (1995).
25. C. L. Hanson, H. Videler, C. Santos, J. P. Ballesta, C. V. Robinson, Mass spectrometry of ribosomes from Saccharomyces cerevisiae: Implications for assembly of the stalk complex. *J. Biol. Chem.* **279**, 42750–42757 (2004).
26. L. Wawiórka *et al*., Functional analysis of the uL11 protein impact on translational machinery. *Cell Cycle* **15**, 1060–1072 (2016).
27. T. M. Schmeing *et al*., The crystal structure of the ribosome bound to EF-Tu and aminoacyl-tRNA. *Science* **326**, 688–694 (2009).
28. J. Spence, S. Sadis, A. L. Haas, D. Finley, A ubiquitin mutant with specific defects in DNA repair and multiubiquitination. *Mol. Cell. Biol.* **15**, 1265–1273 (1995).
29. J. Spence *et al*., Cell cycle-regulated modification of the ribosome by a variant multiubiquitin chain. *Cell* **102**, 67–76 (2000).

30. L. B. Jenner, N. Demeshkina, G. Yusupova, M. Yusupov, Structural aspects of messenger RNA reading frame maintenance by the ribosome. *Nat. Struct. Mol. Biol.* **17**, 555–560 (2010).
31. J. Dong *et al*., Rps3/uS3 promotes mRNA binding at the 40S ribosome entry channel and stabilizes preinitiation complexes at start codons. *Proc. Natl. Acad. Sci. U.S.A.* **114**, E2126–E2135 (2017).
32. Y. Matsuo *et al*., Ubiquitination of stalled ribosome triggers ribosome-associated quality control. *Nat. Commun.* **8**, 159 (2017).
33. C. C. Wu, B. Zinshteyn, K. A. Wehner, R. Green, High-resolution ribosome profiling defines discrete ribosome elongation states and translational regulation during cellular stress. *Mol. Cell* **73**, 959–970.e955 (2019).
34. W. W. Shi, A. N. Mak, K. B. Wong, P. C. Shaw, Structures and ribosomal interaction of ribosome-inactivating proteins. *Molecules* **21**, E1588 (2016).
35. H. P. Harding *et al*., The ribosomal P-stalk couples amino acid starvation to GCN2 activation in mammalian cells. *eLife* **8**, e50149 (2019).
36. A. J. Inglis *et al*., Activation of GCN2 by the ribosomal P-stalk. *Proc. Natl. Acad. Sci. U.S.A.* **116**, 4946–4954 (2019).
37. J. L. Llácer *et al*., Conformational differences between open and closed states of the eukaryotic translation initiation complex. *Mol. Cell* **59**, 399–412 (2015).
38. H. Yamamoto *et al*., Molecular architecture of the ribosome-bound Hepatitis C Virus internal ribosomal entry site RNA. *EMBO J.* **34**, 3042–3058 (2015).
39. S. Martín-Villanueva, A. Fernández-Pevida, J. Fernández-Fernández, D. Kressler, J. de la Cruz, Ubiquitin release from eL40 is required for cytoplasmic maturation and function of 60S ribosomal subunits in Saccharomyces cerevisiae. *FEBS J.* **287**, 345–360 (2020).
40. C. Montellese *et al*., USP16 counteracts mono-ubiquitination of RPS27a and promotes maturation of the 40S ribosomal subunit. *eLife* **9**, e54435 (2020).
41. K. Poncová *et al*., uS3/Rps3 controls fidelity of translation termination and programmed stop codon readthrough in co-operation with eIF3. *Nucleic Acids Res.* **47**, 11326–11343 (2019).
42. V. Balagopal, R. Parker, Stm1 modulates translation after 80S formation in Saccharomyces cerevisiae. *RNA* **17**, 835–842 (2011).
43. D. Simsek, M. Barna, An emerging role for the ribosome as a nexus for post-translational modifications. *Curr. Opin. Cell Biol.* **45**, 92–101 (2017).
44. Z. Shi *et al*., Heterogeneous ribosomes preferentially translate distinct subpools of mRNAs genome-wide. *Mol. Cell* **67**, 71–83.e7 (2017).
45. K. Ikeuchi *et al*., Collided ribosomes form a unique structural interface to induce Hel2-driven quality control pathways. *EMBO J.* **38**, e100276 (2019).
46. S. Juszkiewicz *et al*., ZNF598 is a quality control sensor of collided ribosomes. *Mol. Cell* **72**, 469–481.e7 (2018).
47. S. Manohar *et al*., Polyubiquitin chains linked by lysine residue 48 (K48) selectively target oxidized proteins in vivo. *Antioxid. Redox Signal.* **31**, 1133–1149 (2019).
48. C. Kraft, A. Deplazes, M. Sohrmann, M. Peter, Mature ribosomes are selectively degraded upon starvation by an autophagy pathway requiring the Ubp3p/Bre5p ubiquitin protease. *Nat. Cell Biol.* **10**, 602–610 (2008).
49. M. D. Petroski, The ubiquitin system, disease, and drug discovery. *BMC Biochem.* **9** (suppl. 1), S7 (2008).
50. W. Dröge, Free radicals in the physiological control of cell function. *Physiol. Rev.* **82**, 47–95 (2002).
51. D. Finley *et al*., Inhibition of proteolysis and cell cycle progression in a multiubiquitination-deficient yeast mutant. *Mol. Cell. Biol.* **14**, 5501–5509 (1994).
52. J. Zivanov *et al*., New tools for automated high-resolution cryo-EM structure determination in RELION-3. *eLife* **7**, e42166 (2018).
53. A. Rohou, N. Grigorieff, CTFFIND4: Fast and accurate defocus estimation from electron micrographs. *J. Struct. Biol.* **192**, 216–221 (2015).
54. A. Punjani, J. L. Rubinstein, D. J. Fleet, M. A. Brubaker, cryoSPARC: algorithms for rapid unsupervised cryo-EM structure determination. *Nat. Methods* **14**, 290–296 (2017).
55. Y. Zhou, A. Moscovich, T. Bendory, A. Bartesaghi, Unsupervised particle sorting for high-resolution single-particle cryo-EM. *Inverse Probl.* **36**, 044002 (2020).
56. A. Bartesaghi *et al*., Atomic resolution cryo-EM structure of beta-galactosidase. *Structure* **26**, 848–856.e3 (2018).
57. D. N. Mastronarde, Automated electron microscope tomography using robust prediction of specimen movements. *J. Struct. Biol.* **152**, 36–51 (2005).
58. X. Li *et al*., Electron counting and beam-induced motion correction enable near-atomic-resolution single-particle cryo-EM. *Nat. Methods* **10**, 584–590 (2013).
59. T. Hrabe *et al*., PyTom: A python-based toolbox for localization of macromolecules in cryo-electron tomograms and subtomogram analysis. *J. Struct. Biol.* **178**, 177–188 (2012).
60. M. Eibauer *et al*., Unraveling the structure of membrane proteins in situ by transfer function corrected cryo-electron tomography. *J. Struct. Biol.* **180**, 488–496 (2012).
61. S. Nickell *et al*., TOM software toolbox: Acquisition and analysis for electron tomography. *J. Struct. Biol.* **149**, 227–234 (2005).
62. Y. Chen, S. Pfeffer, T. Hrabe, J. M. Schuller, F. Förster, Fast and accurate reference-free alignment of subtomograms. *J. Struct. Biol.* **182**, 235–245 (2013).
63. F. Förster, R. Hegerl, Structure determination in situ by averaging of tomograms. *Methods Cell Biol.* **79**, 741–767 (2007).
64. F. Brandt, L. A. Carlson, F. U. Hartl, W. Baumeister, K. Grünewald, The three-dimensional organization of polyribosomes in intact human cells. *Mol. Cell* **39**, 560–569 (2010).
65. T. D. Goddard *et al*., UCSF ChimeraX: Meeting modern challenges in visualization and analysis. *Protein Sci.* **27**, 14–25 (2018).
66. P. Emsley, K. Cowtan, Coot: Model-building tools for molecular graphics. *Acta Crystallogr. D Biol. Crystallogr.* **60**, 2126–2132 (2004).
67. P. V. Afonine *et al*., Real-space refinement in PHENIX for cryo-EM and crystallography. *Acta Crystallogr. D Struct. Biol.* **74**, 531–544 (2018).
68. Y. Zhou, A. Bartesaghi, G. M. Silva, Cryo-EM structure of K63 ubiquitinated yeast translocating ribosome under oxidative stress. Electron Microscopy Data Bank. https://www.ebi.ac.uk/pdbe/entry/emdb/EMD-22198. Deposited 20 June 2020.
69. Y. Zhou, A. Bartesaghi, G. M. Silva, Cryo-EM structure of K63R ubiquitin mutant ribosome under oxidative stress. Electron Microscopy Data Bank. https://www.ebi.ac.uk/pdbe/entry/emdb/EMD-22196. Deposited 20 June 2020.
70. Y. Zhou, A. Bartesaghi, G. M. Silva, Cryo-EM structure of K63 ubiquitinated yeast translocating ribosome under oxidative stress. Protein Data Bank. https://www.rcsb.org/structure/6XIR. Deposited 20 June 2020.
71. Y. Zhou, A. Bartesaghi, G. M. Silva, Cryo-EM structure of K63R ubiquitin mutant ribosome under oxidative stress. Protein Data Bank. https://www.rcsb.org/structure/6XIQ. Deposited 20 June 2020.
72. Y. Zhou, A. Bartesaghi, G. M. Silva, Cryo-EM structure of K63R ubiquitin mutant consensus ribosome under oxidative stress. Electron Microscopy Data Bank. https://www.ebi.ac.uk/pdbe/entry/emdb/EMD-22197. Deposited 20 July 2020.
73. Y. Zhou, A. Bartesaghi, G. M. Silva, Subtomogram averaging map of yeast polysome. Electron Microscopy Data Bank. https://www.ebi.ac.uk/pdbe/entry/emdb/EMD-22190. Deposited 29 June 2020.